Article:
Cui, Z, Zhao, J, He, L et al. (2020) A reactive molecular dynamics study of hyperthermal atomic oxygen erosion mechanisms for graphene sheets. Physics of Fluids, 32 (11). 112110. ISSN: 1070-6631

https://doi.org/10.1063/5.0030749

A reactive molecular dynamics study of the surface catalysis and ablation behavior of graphene sheets colliding by hyperthermal atomic oxygens

Zhiliang Cui[1], Jin Zhao[2,1], Lichao He[1], Haichuan Jin[1], Jun Zhang[1], Dongsheng Wen[1,2,3,]**

[1]School of Aeronautic Science and Engineering, Beihang University, Beijing, 100191

[2]School of General Engineering, Beihang University, Beijing, 100191

[3]School of Chemical and Process Engineering, University of Leeds, Leeds, LS2 9JT

Abstract

Carbon-based composite materials, whose mechanisms of surface catalysis and ablation during the impact of oxygen atoms remain unclear, are widely used in the aerospace field due to their light weight, ideal physical and chemical properties. In this study, the surface catalysis and ablation behaviors during the erosion process of hyperthermal atomic oxygens was investigated by molecular dynamics (MD) simulation method with ReaxFF potential. Seven models were established to study the impact of the energy flux density for the energetic oxygen atoms, the presence of multiple layers beneath the graphene sheet, and the effect of three different graphite surfaces, namely graphite basal plane, armchair edge surface and zigzag edge surface, respectively. The simulation results show that for all the seven models, the adsorption of oxygen atoms dominates at the beginning for all models, generating O_2 molecules through the surface catalytic recombination effect. The ablation rate of graphene surface accelerates significantly as oxygen energy flux density increases due to the higher system temperature. The multi-layered graphite slab can be etched by hyperthermal atomic oxygen with a 'layer-by-layer' phenomenon. The more graphene stacks appearing below the top layer, the slower the ablation rate due to the fact that additional graphene layers can act as a heat sink to slow down the temperature rise by conduction due to oxygen-atom collisions. Graphite surfaces with AC surfaces show the largest

etching rate and basal presenting the lowest etching rage, revealing the fact that the binding energies of the AC edge tends to be weaker than those of the ZZ edge, causing that the AC surface model is difficult to form stable functional group structures to resist the etching of high-energy oxygen atoms than the ZZ surface. This research advances our understanding of the detail surface catalysis and ablation mechanisms during the erosion process of graphene sheets from the prospective of atomistic scale.

Keywords

Reactive Molecular dynamics (RMD) simulation, hyperthermal atomic oxygens, surface catalysis and ablation, graphene sheet

1 Introduction

Carbon-based materials have been applied as heat shields in spacecraft applications due to their desirable physical and chemical properties [1, 2]. At low-earth-orbit (LEO) altitude, the dominant component of this rarefied atmosphere environment is atomic oxygen with a number density of around 10^{15} atoms/m^3. This atomic oxygen density, for instance, with a combination of the orbital velocity of 8 km/s for the spacecraft would yield an oxygen flux of 10^{19} atoms/(m^2·s) at a mean collision energy of 5 eV [3]. Thermal protection materials would undergo complex physical and chemical response to such conditions including surface catalysis and ablation reactions [4-7]. Aiming to identify the material damage and characterize the aerodynamic heating due to the collisions of hyperthermal atomic oxygens accurately, a fundamental understanding of the surface catalysis and ablation reaction mechanisms for carbon-based materials is essential for thermal protection system design of with space based applications.

Recent experimental works using multi-scale imaging techniques have provided valuable information for such a high-energy collision process with a focus on carbon-based material surfaces. Murray et al. [8, 9] conducted hyperthermal scattering experiments of both atomic oxygen (O) and molecular oxygen (O_2) collisions on High

Orientation Pyrolytic Graphite (HOPG) surfaces to reveal the mechanisms of carbon oxidation over a wide temperature range. Nicolson et al. [10] further reported the effect of temperature on corrosion rate and surface roughness. These experimental results indicated that the ablation rate of graphite was more dependent on the graphite surface temperature, which was controversial with other experimental conclusions [11-13] implying the exposure impacts of atomic oxygens. From the perspective of experimental design, many of key process parameters are closely interrelated, such as temperature, pressure and energy flux of incoming atomic oxygens, making it challenging to change one only while keeping others unchanged, which in turn makes an identification of the key mechanism difficult. In parallel with these experimental research, theoretical investigations aimed at understanding the surface catalysis and ablation process of carbon-based materials upon hyperthermal oxygen atom collision have also been carried out in the past. Arrhenius type expressions have been excessively applied to fit with the experimental reaction rates, while the possible physiochemical mechanism insights are still hard to achieve aiming to serve as a fundamental guide to design materials.

Density Functional Theory (DFT) based modelling has been shown its capability of providing such detailed physical and chemical information during the interactions between carbon element and energetic atomic/molecular oxygen. Studies on the interaction between graphite surface and high-energy oxygen atoms [14-17] reported that oxygen molecules were generated during the collisions due to the surface catalysis effect through the Eley-Rideal (E-R) mechanism, which was much more important than the Langmuir-Hinshelwood (L-H) mechanism. The formation mechanism of CO and CO_2 was further investigated with DFT method by Paci et al. [18-21], reporting that oxygen atoms were adsorbed on the graphite surface to form epoxy functional groups firstly, which were then diffused to form ketone groups or carbonyl groups, resulting different formation of CO and CO_2. It can be found that these ab initio simulations based on DFT can provide accurate information during the physical interaction and

chemical reaction processes, but their associated computational cost limits their applicability to systems with sizes of only a few angstroms and time scales of a few picoseconds.

With rapid advances in high-performance computing systems in the last few decades, the classical Molecular Dynamics (MD) simulations have shown their abilities to simultaneously model large system sizes for a long time. Thus MD method has been recently employed to study the mechanical and thermal properties for graphite and graphene materials [22-24] and their complicated physical interactions with other species [25, 26] at the atomistic level. These MD simulations, however, have not elucidated the chemical reaction mechanisms. With the continuous development of force field potentials, an empirical reactive potential ReaxFF was recently proposed by van Duin et al. [27] to simulate the physics, chemistry and dynamics of various processes for graphitic materials [28-30]. Poovathingal et al. [31] studied the oxidation of hyper-thermal oxygen atom beams with HOPG based on reactive molecular dynamics (RMD). The simulation predicted that the composite reaction occurred on the graphene sheet, but the carbon removal reaction only occurred on the edge of the corrosion pit. Srinivasan et al. [32] simulated the ablation process of high-energy oxygen atoms colliding with the diamond surface in a low-earth orbit (LEO) environment, observing that a variety of functional groups such as ethers, peroxides, oxygen radicals and dioxins were formed on the diamond surface. Ermakov et al. [33] later performed a simulation process of exposing three layers of graphene to atomic oxygen, and reported that the graphene gasified uniformly layer by layer. Majumder et al. [34] studied the energy transfer when O_2 collided with the graphite surface. It is found that the average energy transferred to the graphite surface and the average energy retained in the O_2 translation were linearly related to the initial translation energy. Liu et al. [35] simulated the bombardment of single-layer graphene films by different energetic atoms. The results showed that the incident energy played an important role in the evolution and final shape of graphene defects. Bai et al. [36] systematically

explored the effects of incident angle and incident energy on defects and vacancies by using molecular dynamics with reactive force fields. It is found that oxygen ions with an incident angle of 70° showed the highest ion replacement rate. Qiao et al. [37] fine-tuned the theoretical graphene oxide (GO) model based on RMD simulations and experimental characteristics. The scattering process of N_2 impinging on graphite was also simulated to investigate the effects of angular distribution of N_2, the average translational energy and rotational energy, and the number of rebounds [38, 39]. It also reported the simulation of other materials impacting graphite, exploring the effects of nickel pellets on graphene at the supersonic velocity, and the dynamics of H_2O, CO_2, and glycine (GLY) colliding with graphite [40-42]. These RMD simulations suggest that ReaxFF potential allows for the simulation of chemical reactions on large systems while retaining most of the accuracy of DFT, which can be used as an effective tool to screen and characterize materials for applications in extreme environments.

Though previous RMD studies have advanced our understanding of the collisions between atomic oxygen and graphitic materials, the surface catalysis and ablation mechanism still remains unclear due to its complex physiochemistry nature during this gas-solid interaction process. In this work, RMD simulation method with ReaxFF reactive force field has been employed to gain an atomically detailed understanding through seven independent models with a twofold purpose, firstly using Model I to demonstrate the suitability of the choice of ReaxFF force field and calculation set-up, and secondly to further apply this approach to obtain a deeper understanding of the catalytic and ablative reaction process when the graphene is exposed to hyperthermal atomic oxygen collisions: The impact of the energy flux density for the energetic oxygen atoms is investigated; In addition, a study of the effect of the presence of multiple layers beneath the graphene sheet is carried out; Finally, the effect of three different graphite surfaces is examined, namely graphite basal plane, armchair edge surface and zigzag edge surface, respectively. A detailed description of the computational methods and model constructions is presented in section 2, followed by

a discussion of the results in section 3 and conclusions in section 4.

2. Molecular Dynamics Simulation Details

2.1 ReaxFF Reactive Force Field Method

The ReaxFF reactive force field [27] were applied to investigate the hyperthermal collisions of atomic oxygen with graphene in the present work. ReaxFF is a general transferrable bond-order (BO) based empirical potential that uses relationships between bond distance and bond order on the one hand, and relationships between bond order and bond energy E_{bond} on the other to describe bond formation and bond dissociation properly. The system energy E_{sys} in ReaxFF is calculated as the sum of a number of energy terms according to

$$E_{\text{sys}} = E_{\text{bond}} + E_{\text{val}} + E_{\text{tors}} + E_{\text{vdWaals}} + E_{\text{Coulomb}} + E_{\text{lp}} + E_{\text{over}} + E_{\text{under}} + E_{\text{pen}} + E_{\text{conj}} \quad (1)$$

where the valence angle energy E_{val} and torsion angle energy E_{tors} are made functions of bond order so that their energy contributions go to zero smoothly upon bond dissociation; Non-bonded interactions, including intermolecular van der Waals potential E_{vdWaals} and electrostatic interaction potential energy E_{Coulomb}, are calculated between every atom pair, irrespective of the connectivity; And other correction terms, including energy compensation terms related to lone pair electrons E_{lp}, over-coordination energy E_{over}, under-coordination energy E_{under}, compensation function E_{pen}, and four-body conjugation energy E_{conj}, are used to describe the fracture and formation of chemical bonds in different chemical environments properly. Excessively short range interactions are avoided by using a shielding term in the energy expression for the nonbonded interactions. Instead of Ewald summation to calculate long-range Coulomb interactions, ReaxFF uses a seventh-order taper function with an outer cutoff radius of 10 Å.

The force-field parameters used in the present simulations were extended by Chenoweth et al. [43] as ReaxFF$_{\text{C/H/O}}$, which was parameterized against an extensive

training set consisting of atomic charges, bond lengths, valence and torsion angle energies, heats of formation and various hydrocarbon reaction energies. A detailed description of the data included in the parameterization of $ReaxFF_{C/H/O}$ formulation can be found in the original work. $ReaxFF_{C/H/O}$ has been successfully used to study the oxidations of graphene, graphite and diamond subject to high energy oxygen atom bombardment, which results show a good agreement with earlier experiments and first-principle-based calculations [44].

2.2 Model Construction

Firstly, to verify our simulations, a careful benchmarking of the approach was established aiming to reproduce the results of Srinivasan et al. [44], as a reference Model I shown in **Figure 1(a)**. Model I had a graphene sheet with a total of 384 carbon atoms, where the dimensions of the graphene basal plane were 34.10 Å×29.53 Å in the *x*- and *y*-axis directions. The impinging atomic oxygen was initially generated every 1.0 ps at a vertical separation of 5.0 Å above the graphene basal plane, whereas the in-plane coordinates were chosen randomly. The graphene sheet was subjected to collide by these oxygen atoms with their translational energies of 5 eV, which value was also considered as the mean energy when oxygen atoms hit the spacecraft in low-Earth orbit [3]. To ensure that the leaving species after collision did not interfere the surface chemistry, the *z* dimension of the unit cell was chosen to be 240 Å. Periodical boundary conditions were used in the directions parallel to the graphene basal plane, while the reflective boundary condition was used in the z-axis direction. To avoid the downward displacement of the graphene sheet due to the continuous bombardment by hyperthermal atomic oxygens, the positions of carbon atoms at each corner of the graphene sheet were fixed to ensure that the center of mass of the graphene in the z-axis direction was remaining stable.

Three sets of ReaxFF-based MD simulations, comprised of seven independent models, were carried out, as presented in **Figure 1**. The first set of simulations investigated the effect of energy flux density for the impingement of the hyperthermal

atomic oxygens on the reactive events: Through keeping the same impinging energy of the hyperthermal oxygen atoms as Model I, the particle flux in Model II and III was decreased by expanding the graphene sheet structure along each of the coordinate directions of the basal plane by 1.5 and 2 times, respectively. Thus, three different energy flux densities ξ of the impinging atomic oxygens were studied in these simulations, which were calculated as a result of 1.590, 0.707 and 0.397 MW/cm^2, respectively. **Figure 1(b)** and **1(c)** shows the expanded sheets, having a total of 864 and 1536 carbon atoms. The second set of simulations involved the effect of the presence of multiple layers beneath the graphene sheet on the surface catalysis and ablation process. Two-layer and six-layer graphene stacks in the AB arrangement with an interlayer distance of 3.2 Å [44] were established as shown in **Figure 1(d)** and **1(e)**, denoted as Model IV and V. The carbon atoms are colored in blue and red to distinguish them among different layers. The third set of simulations investigated the continuous bombardment outcome of graphite with different edges by hyperthermal atomic oxygen. Through advancing Model V as a standard graphite basal plane, Model VI and Model VII were built up where the graphite armchair edge and zigzag edge of a model graphite were exposed to hyperthermal oxygen atom collisions normal to the surface, as presented in **Figure 1(e, d, f)**.

All the systems were energy-minimized before being used for MD simulations with the LAMMPS package. A time step of 0.10 fs was used for all simulations with the microcannocial (*NVE*) ensemble, because a local increase in temperature along the time due to the collision event is essential in driving the surface catalysis and ablation reactions [44]. A total of 500 ps simulations was conducted for all the models, except for Model I with only 200 ps calculations, as the graphene sheet was shown to get broken into fragments by then. The trajectories of each atomic species for each system were collected every 0.10 ps for all the post-processing process. More information of model construction details in this work can be found in the **Supplementary Material**.

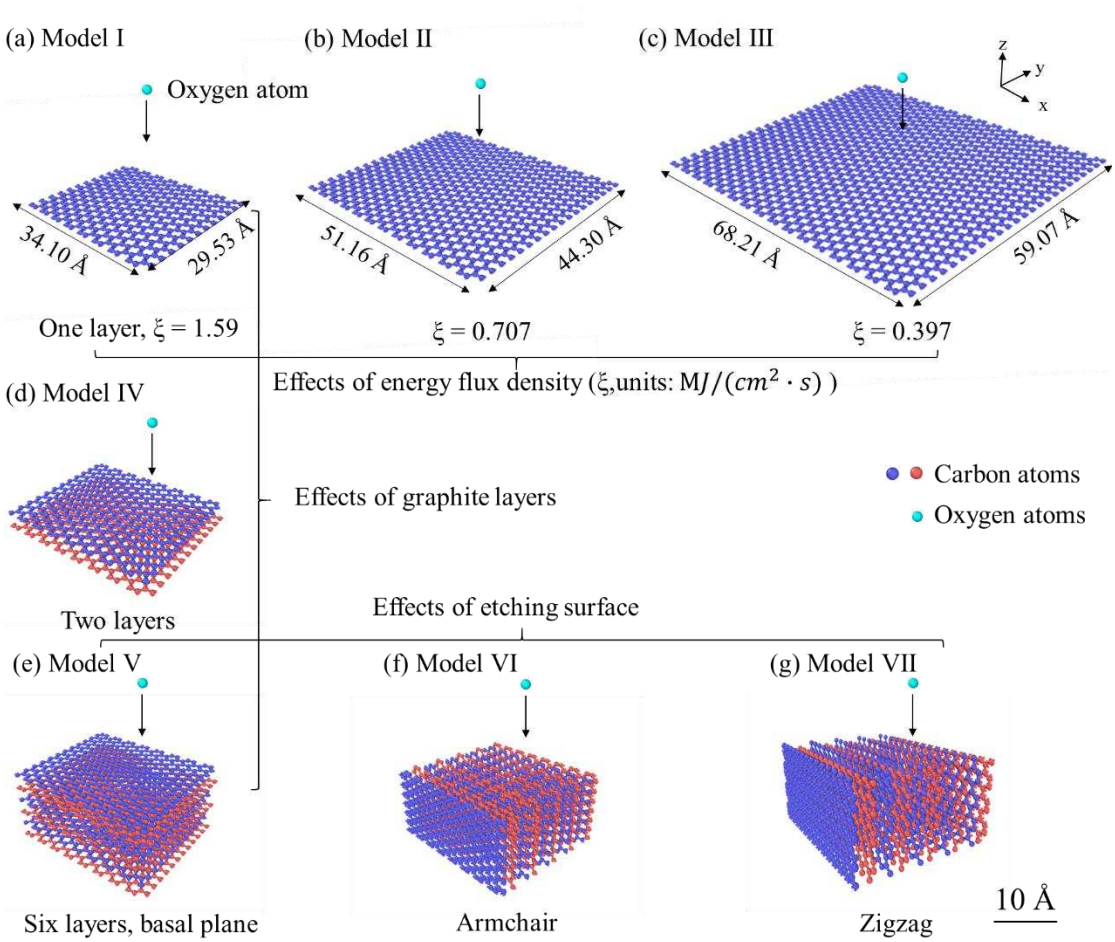

Figure 1 The schematic illustrations of initial configurations for the simulated systems

3. Results and Discussion

Section 3.1 discusses the validity of the choice of ReaxFF$_{C/H/O}$ force field and MD calculation set-up through a benchmark case investigation of Model I. Section 3.2, 3.3 and 3.4 report the physical/chemical interactions between the hyperthermal atomic oxygens and the solid surface with the effects of the oxygen energy flux density ξ with 1.590, 0.707 and 0.397 MW/cm^2, the presence of multi layers beneath the graphene sheet surface (a total of 1/2/6 layers) and the graphite surfaces with different edges (graphite basal plane surface, armchair edge surface and zigzag edge surface).

3.1 A benchmark case for validation

As mentioned previously, the validation of our simulations is demonstrated by a careful benchmarking of the approach on Model I aiming to reproduce the results of Srinivasan et al. [44]. The evolution of reaction events leading to the breakup of the

graphene sheet is illustrated in **Figure 2(a)**, which is compared with that of Srinivasan et al. [44]. It can be observed that in the time period from 0 to 40 ps, the impinging oxygen atoms are adsorbed and bind onto the surface in the forms of epoxide. The hole-shape defects in the sheet can be visualized at a snapshot of 80 ps from the simulation results. With rapid development of the defect formation and growth, the graphene sheet is broken into fragments by 100 ps. This process shows a good agreement with that of Srinivasan et al. [44] presented in **Figure 2(b)**, indicating the validity and stability of our calculation setup.

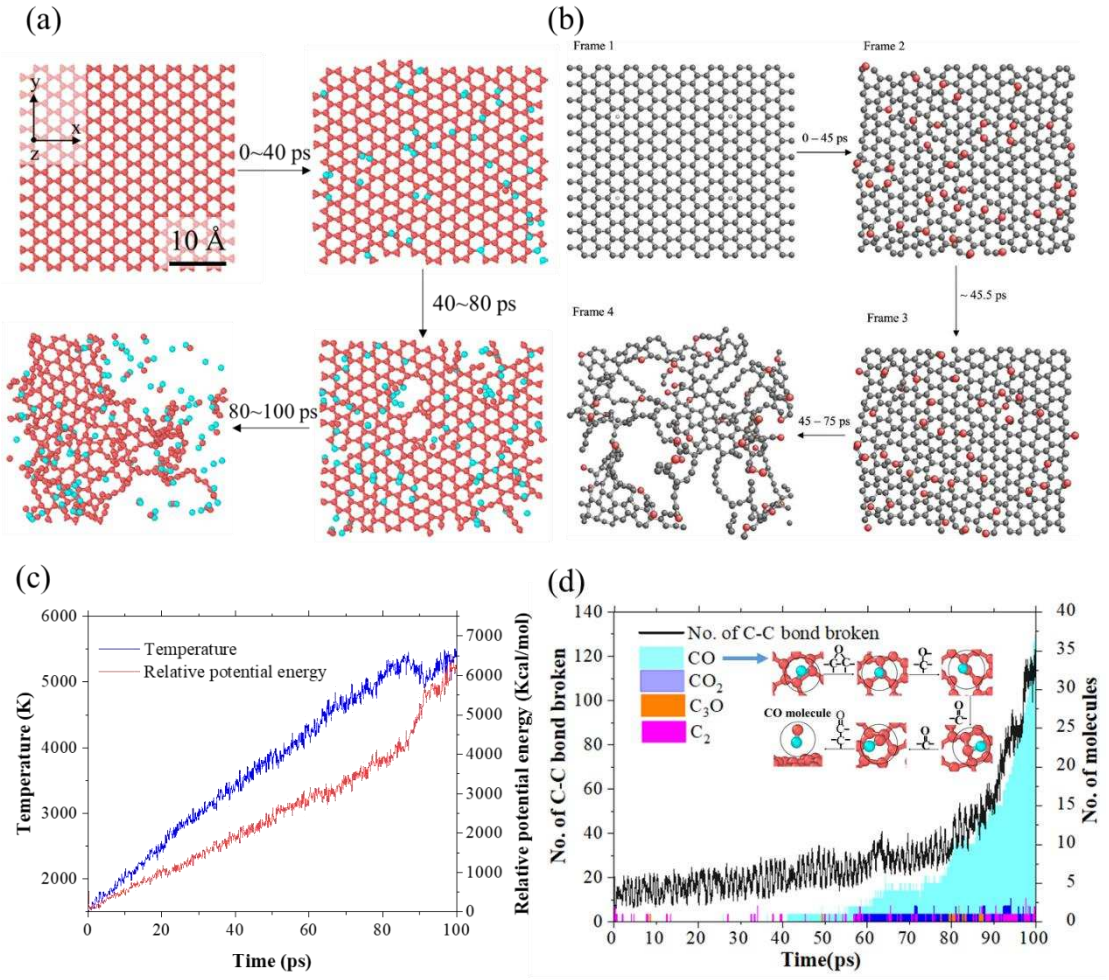

Figure 2 The detail simulation results of Model I. ((a) The breakup process of the graphene sheet due to successive atomic oxygen impacts (Carbon atoms are colored red and oxygen atoms are colored cyan) with (b) a comparison of the result from Srinivasan et al. [44]; (c) Variations of system temperature and potential energy for Model I; (d) Number of C-C bond broken and the product analysis as a function of time with an illustration of the formation process of a CO molecule)

During the continuous impingement of atomic oxygens, both the temperature and

the relative potential energy (relative to that of the pristine graphene sheet) increase, as depicted from **Figure 2(c)**. It should be noted that the system temperature remains approximated stable from 80 to 100 ps, accompanied with a sharp rise in the potential energy. This indicate that most of the energy input to the system through the addition of successive oxygen atom impacts is consumed by breaking the carbon-carbon (C-C) bonds of the graphene sheet. The evidence can be quantitatively observed from the significant increase of the C-C bond broken number variation as a function of time in **Figure 2(d)**, where an interatomic distance of less than 1.8 Å between two carbon atoms is applied as a criterion for the C-C bond breakage for the graphene film structure [44]. The statistics of all the gas species leaving from the graphene sheet are obtained as also shown in **Figure 2(d)**. It can be found that the dominant products during the reaction process are CO molecules, where the generation and release process of a CO molecule is illustrated in **Figure 2(d)**. The production of CO is monitored to occur due to the epoxide formation, migration and ring-opening reactions. A small number of CO_2 molecules are observed after around 57 ps, with some C_2 and C_3O as intermediate products.

3.2 The effect of impinging energy flux density on the graphene erosion

The impinging energy flux density effect of hyperthermal atomic oxygens on the erosion process of a graphene sheet is reported in this section, which is 1.590, 0.707 and 0.397 MW/cm^2, respectively. This is implemented through expanding the graphene sheet structure in Model I by 1.5 and 2 times, respectively, along each of the coordinate directions of the basal plane to decrease the particle flux, while keeping the same impinging energy of the hyperthermal oxygen atoms as Model I. Thus, three different energy flux densities ξ of the impinging atomic oxygens were studied in these simulations, which were calculated as a result of 0.397 MW/cm^2 for Model III, 0.707 MW/cm^2 for Model II and 1.590 MW/cm^2 for Model I, respectively.

Figure 3(a) illustrates the snapshots of Model II with evolutions of time from 0 to

300 ps. It can be observed that, as the impinging energy flux density decreasing from 1.590 MW/cm^2 to 0.707 MW/cm^2, the breakup rate of Model II seems to be delayed but still following the same erosion procedure with Model I: The adsorption behavior of atomic oxygens onto the graphene sheet is dominant with the formation of epoxides from 0 to 100 ps; Some hole-shape voids/defects in the sheet can be visualized at a snapshot of 100 ps; The graphene sheet is rapidly broken into fragments by 200 ps with the development of defect formation and growth, following by completely destroyed by 300 ps.

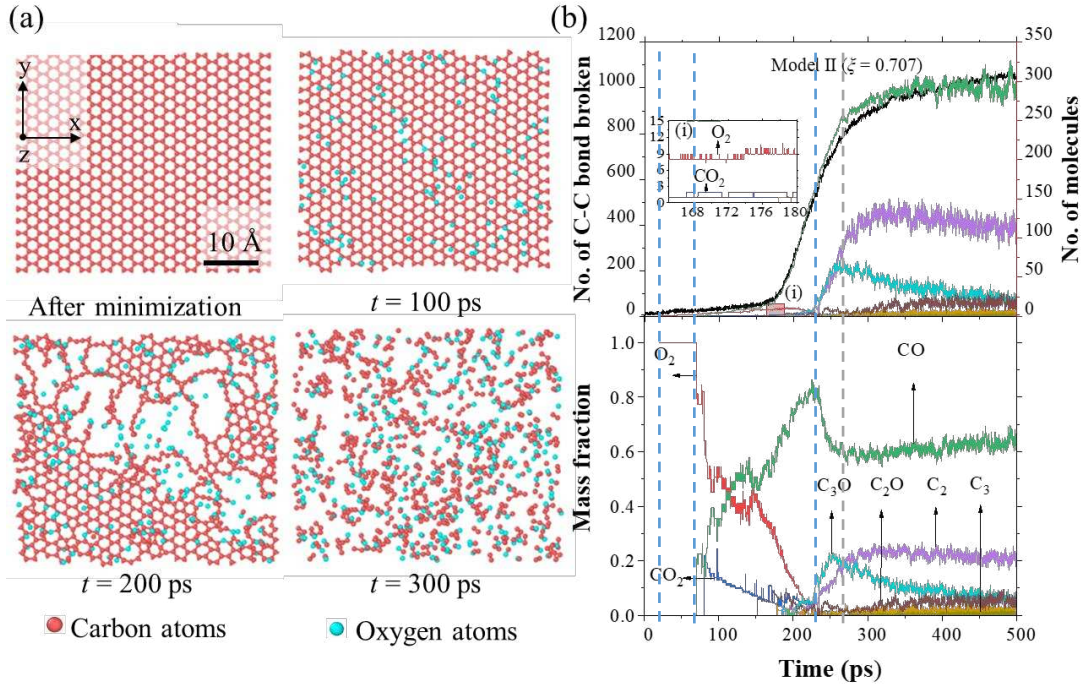

Figure 3 The erosion process of graphene sheet with energy flux densities ξ=0.707 MW/cm^2 of the impinging atomic oxygens. (a) the snapshot illustrations of graphene sheet with the evolution of time (b) the gas species analysis during the erosion process

To further analyze the erosion process of Model II with the incoming energy flux density of 0.7 MW/cm^2, the C-C bond breaking analysis, the number of generated gaseous species and their corresponding mass fractions are quantified as plotted in **Figure 3(b)**. The formations of the gaseous species are summarized more than those similar compounds of CO, CO_2, C_2, and C_3O observed by Srinivasan et al. [44]. Dominant O_2 molecules amongst all the gaseous species are observed incipiently from

around 20 ps: (1) At Stage 1, though a few C-C bonds on the graphene sheet are broken, there is no gaseous species releasing from the graphene sheet before around 20 ps; (2) At the second stage, only O_2 molecules are released approximately from 20 to 70 ps, resulting in whose corresponding mass fraction of 1 (100%); (3) Both CO and CO_2 molecules are formed (thereby creating vacancy defects on the graphene sheet) during this third stage of this erosion process, which is also accompanied by rapid consumption of O_2 molecules. The number of the broken C-C bonds for the graphene sheet trends to increase exponentially from around 170 ps. Moreover, almost all the O_2 molecules are consumed at around 220 ps, along with few CO_2 oxidation products are generated afterwards. At this point, the CO molecule becomes the dominant gaseous production with its corresponding mass fraction plot reaches to its peak value of 0.86 (86%). An instance of C_2, C_3, C_2O and C_3O formations can also be monitored at this stage; (4) At Stage 4, the CO yield is monitored to be dominant due to the epoxide formation, migration and ring-opening reactions, where with C_3O and C_2 molecules to a less extent by 270 ps. (5) Finally, with further successive oxygen impingement, a 60% mass fraction of CO molecules and 20% of C_2 molecules are becoming the main composition, accompanied with a remaining small number of C_3, C_2O and C_3O formations.

The quantitative analyses of generated gaseous species number and their corresponding mass fractions with evolutions of time for Model I and III with the incoming energy flux density of 1.590 and 0.397 MW/cm^2 are summarized and plotted in **Figure 4(a, b)**. Compared with Model II in **Figure 3(b)**, the trends of the number of C-C bonds broken, the number of each production molecules and their mass fraction for Model I, III are consistent, while the whole erosion process occurs faster for Model I and slower for Model III. The formation of O_2 molecules are also monitored incipiently for both Model I and III. Through capturing the trajectories of O_2 formation procedures, it can be found that the formation of O_2 molecules are resulted from the surface catalytic recombination effect with both E-R and L-H mechanisms. As illustrated with the snapshots in **Figure 4(c)**, some O_2 molecules are formed by one

adsorbed oxygen atom on the graphene surface recombining with another atomic oxygen from the incoming particle flux due to the collisions, as known as E-R mechanism; there are also some O_2 molecules formed by the recombination of two adsorbed atomic oxygens binding onto the graphene surface due to the diffusions, called L-H mechanisms. It can be noticed that the formation of O_2 molecules due to the surface catalysis effect is closely related with the incipient adsorption of atomic oxygens onto the graphene sheet surface. Therefore, the z-density plots of atomic oxygens as a function of time for Model I ~ III are summarized in **Figure 4(d)**. It can be observed that with the decrease of the impinging energy flux density from 1.590 to 0.397 MW/cm^2, the adsorption period of the atomic oxygens onto the graphene surface is extended obviously. For instance, when the impinging energy flux density decreases to 0.397 MW/cm^2 (Model III), the number of adsorbed atomic oxygens remains relatively stable from 50 to 100 ps, following by a trend of descent from 100 to 150 ps due to the surface catalysis recombination effect and then releasing from the surface.

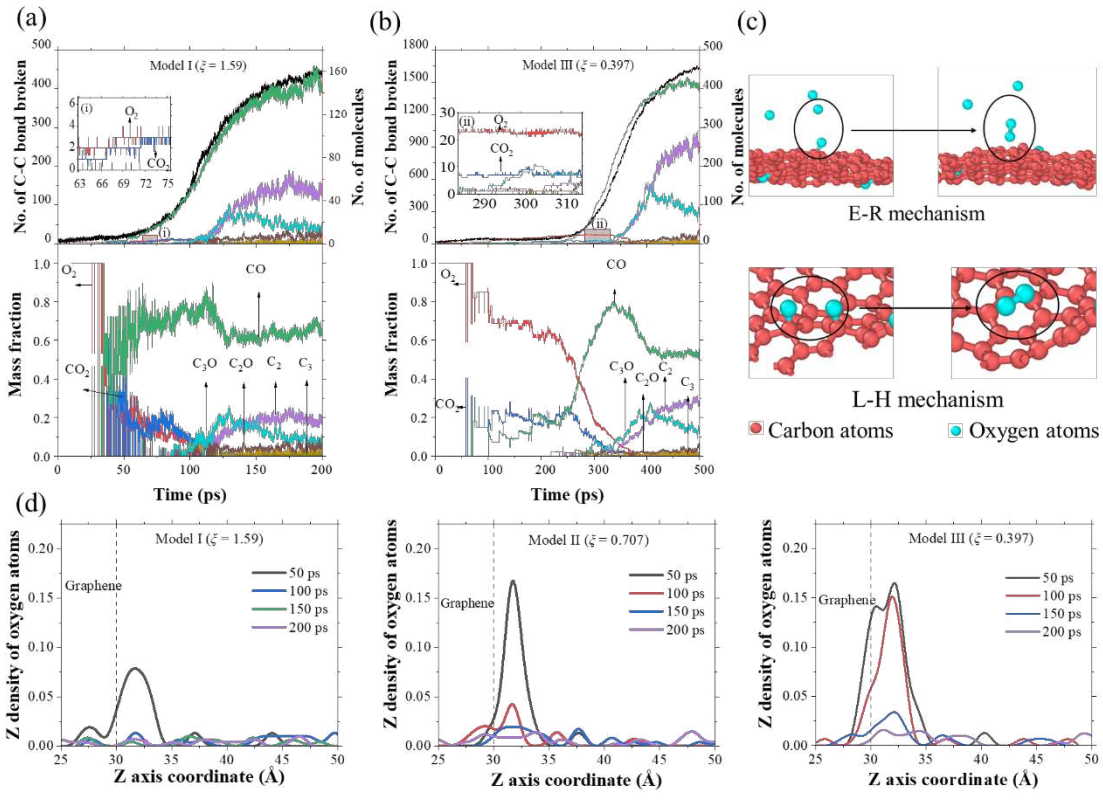

Figure 4 The gas component and z-density analysis during the oxygen impingement

for models with different energy flux densities of the atomic oxygens.

A comprehensive comparison for the effect of incoming energy flux density on the surface catalytic and ablation processes for Model I, II, and III is shown in **Figure 5**. The system temperature profile and the fraction of C-C bond broken profile for each graphene sheet are presented in **Figure 5(a)**. Within the procedure of the NVE simulation of the graphene sheet, the system temperature profiles for all the three models with different incoming energy flux density of atomic oxygens are ascending continuously, which is attributed to these incoming hyperthermal atomic oxygens input to the system. As a result, at the same impingement time, the graphene temperature is much higher for the case with greater energy flux density of the impinging oxygen atoms, which leads to a greater erosion rate, as shown in the C-C bond breaking fraction profiles. The inset snapshots of the graphene surface at the time of 200 ps for Model I ~ III shown in **Figure 5(a)** indicate that a severer erosion process can be achieved with greater energy flux density of oxygen atoms colliding with the graphene sheet.

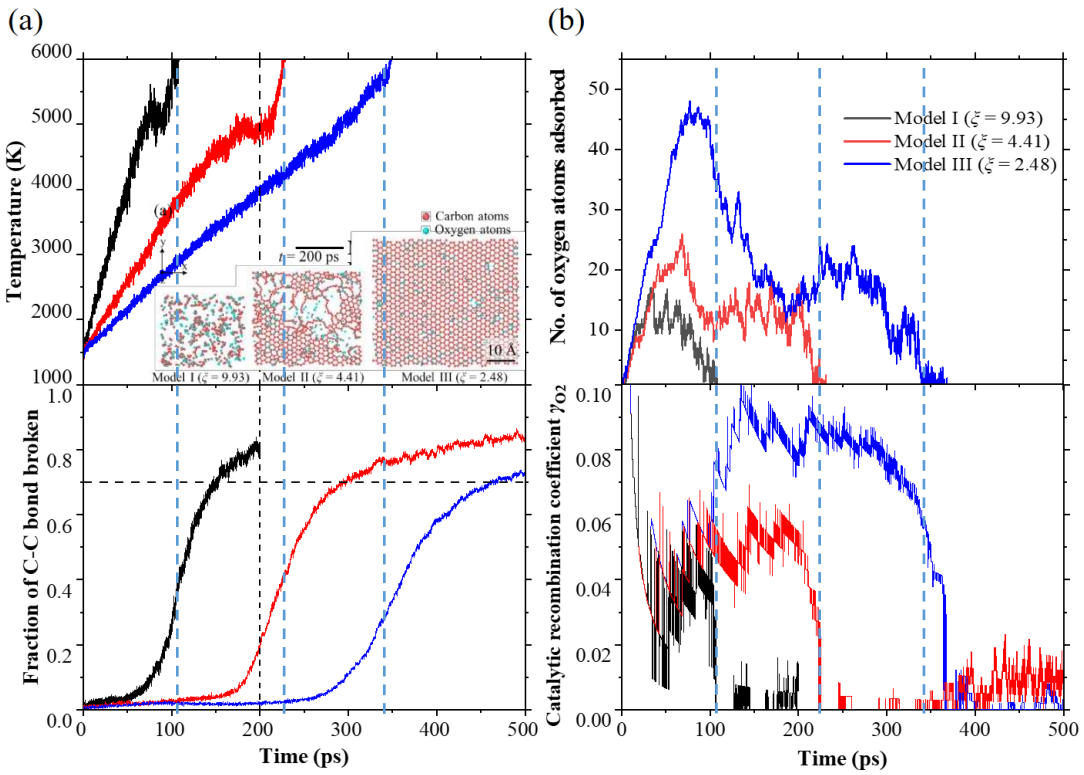

Figure 5 A comprehensive comparison for the effect of incoming energy flux density on the surface catalytic and ablation processes for Model I, II, and III. (a) The system

temperature with the snapshot illustrations for Model I, II, III at 200 ps, along with the Fraction of C-C bond broken as a function of time. (b) the number of adsorbed oxygen atoms on the graphene surface and corresponding catalytic recombination coefficient as a function of time.

To further identify the surface catalysis process for the O_2 formations, the number of oxygen atoms adsorbed onto the graphene sheet and the corresponding recombination coefficient profiles are shown in **Figure 5(b)**. The recombination coefficient γ_{O_2} is defined to quantify the surface catalysis process as the fraction of impinging atoms that recombining to O_2 molecules at the graphene surface. The results indicate that the recombination coefficient is highly dependent on the energy flux density of incoming oxygen atoms, which is closely related to the surface temperature.

The surface catalytic recombination coefficient γ_{O_2} for Model III with the smallest energy flux density of 0.397 MW/cm^2 is the shown to be largest with an average value of 0.081, which results is controversial to a traditional linear-like Arrhenius fit with the monotonically increasing correlation model between surface temperature and surface catalytic recombination coefficient. Our result can indicate that the traditional Arrhenius expression for the surface catalytic recombination coefficient as a function of temperature may only be valid within a certain temperature range. Since the system temperature range to evaluate the surface catalysis can be as great as 6000 K for all the three cases in this study, the average surface catalytic recombination coefficient is found to decrease when the energy flux density is increased from 0.4 to 1.6 MW/cm^2 due to the effect of severe ablation concurrence. To further address this point, another Model 1S with the energy flux density of 0.07 MW/cm^2 has been simulated with more detail results providing in the **Supplementary Material**, where the average surface catalytic recombination coefficient for Model 1S is calculated to be a value of 0.041.

3.3 The erosion process of multilayer graphene films

To investigate the effect of multilayer graphene films on the erosion process, the bombardments of graphene stack with 2 and 6 layers (or graphite in general) in the AB arrangement with hyperthermal atomic oxygens are examined in this section through Model IV and V in comparison with the one-layer graphene sheet of Model I.

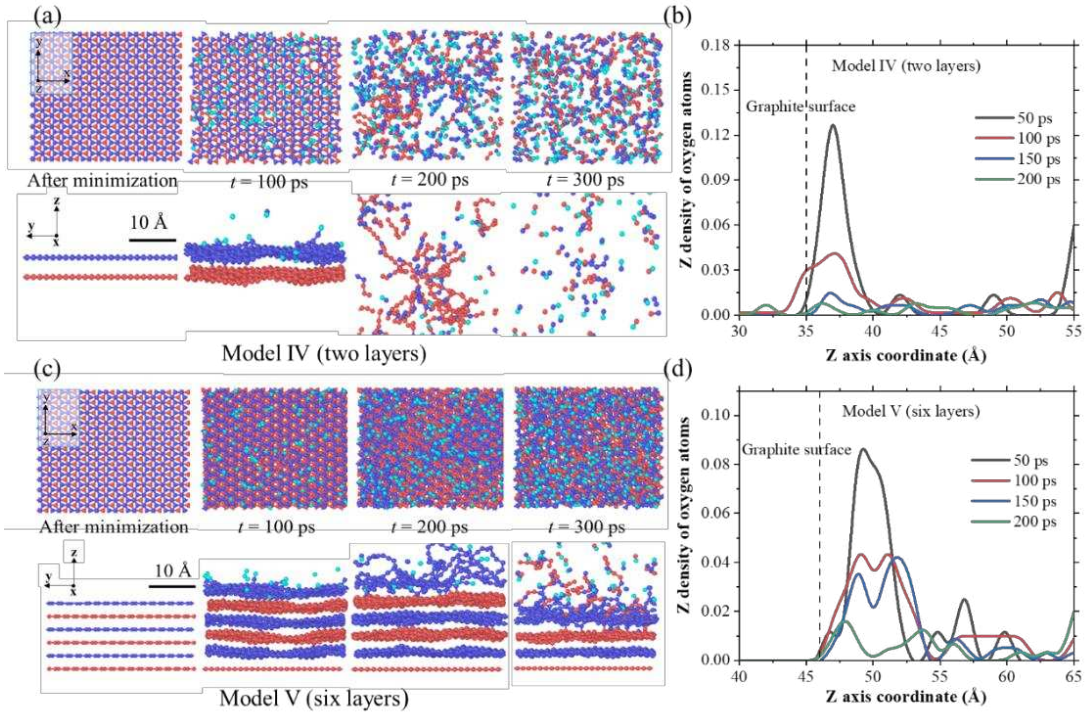

Figure 6 The snapshot illustrations of Model IV and V with oxygen z-density analysis with the evolution of time.

Figure 6 illustrates the snapshots of the erosion processes for Model IV and Model V from both top and side views with the evolution of time from 0 to 300 ps. For both models, graphite erosion proceeds firstly through atomic oxygens adsorb on the graphene stack surface with the formation of epoxides, as shown in the peaks of oxygen z-density profiles in the early stage as presented in **Figure 6(b, d)**. Then, The growth of vacancy defects on the top layer surface, followed by the same procedure on the subsequent layer below. The breakup of graphite for both models is observed to be a layer-by-layer event with the growth rate of defects much larger along the basal plane directions compared to the axial direction. Our result is consistent with that of Srinivasan et al. [44], reporting that the second layer began to be etched when the

carbon atoms in the top layer were almost completely consumed. This phenomenon is proved by the qualitative trends of the C-C bond broken number plot as a function of time, as shown in **Figure 7(a)**. Eventually, the number of broken C-C bonds for all the layers reach the same maximum value, indicating that the graphene layer is completely broken at this time. The leaving population and mass fraction for each gas composition during the reaction for both models are obtained as shown in **Figure 7(b)**, which trends are similar with the single-layer models (Model I~III) as shown in **Figure3(b)** and **Figure 4(a, b)**. The gas phase are populated initially with O_2 and CO_2 molecules due to the surface catalysis and oxidation reactions, respectively. Later, as the system temperature increasing, CO and C_2 dominates among all the leaving gas species. The recombination coefficients and fraction of C-C bond broken for multilayer graphene models are derived from these and presented in **Figure 8(b)**.

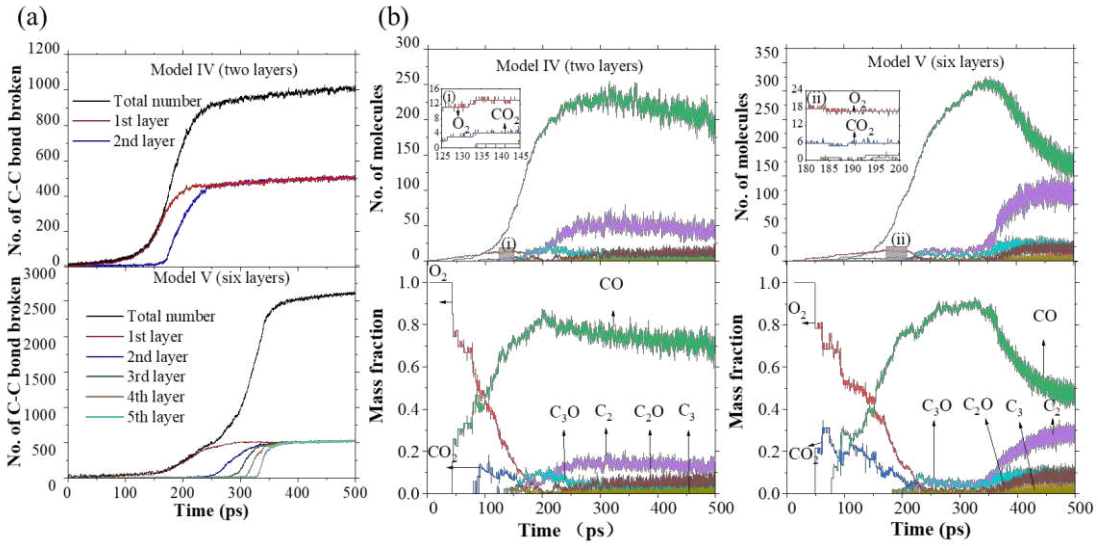

Figure 7 The C-C bond broken profiles and gasified component analysis as a function of time for Model IV and V over time.

Additionally, it should be noted from **Figure 7(a)** that, the C-C bond broken of the top layer (1st layer) for Model V is slower than that of Model IV. In the meanwhile, the ablation rate for Model V with six graphene layers is the slowest as shown in **Figure 8(b)**, compared with the single-layer Model I and two-layer Model IV. This is because that, compared with Model IV, more graphene stacks appearing below the top layer in

Model V, acting as a heat sink that slows down the temperature rise by conduction due to oxygen-atom collisions. The temperatures of Model I and IV both exceed 6000 K at 200ps with Model I almost completely broken (~80% C-C bond broken) and Model IV partially broken (~60% C-C bond broken), while the temperature of Model IV is around 3500 K with the model slightly ablated (~10% C-C bond broken) as shown in **Figure 8 (a, b)**.

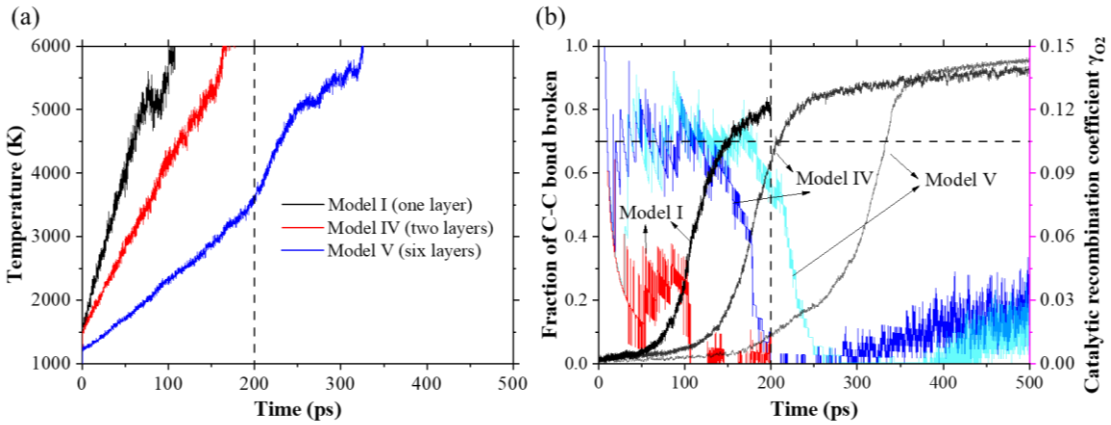

Figure 8 The system temperature profiles and the surface catalysis / ablation analysis as a function of time with the comparisons of Model I, IV and V.

3.4 Graphite surface effects on the atomic oxygen erosion process

To quantifying the effect of the graphite orientation on the surface catalysis and oxidative erosion rates, the simulation results of Model V, VI, VII are compared in this session with graphite basal plane, armchair (AC) edge surface and zigzag (ZZ) edge surface exposing to energetic oxygen atom collisions normal to the surfaces.

A sequence of states through which graphite surfaces with armchair (Model VI) and zigzag (Model VII) conformations proceeding upon hyperthermal atomic oxygen collision is illustrated in **Figure 9**, associating with the z-density profiles of oxygen atoms as a function of time. Combining with the graphite basal plane of Model V, successive oxygen atom collisions indicate that all the three surfaces can be etched by hyperthermal atomic oxygens. The breakup of the graphene stack happens through a layer-wise sequential erosion process. Taking Model VI with armchair surface as an

example, from the initial state to 100 ps, the z-density peaks of oxygen atoms near the graphite surface in **Figure 9(b)** indicate the dominant adsorption behavior of oxygen atoms on the graphene surface. Moreover, z-density of oxygen atoms in Model VII is greater than that in Model VI from 0 ps to 200 ps, as shown in **Figure 9(b, d)**. Compared with Model VI with AC surface, Model VII with ZZ surface is ablated more slowly compared with Model VI and its structure at around 300 ps becomes chaotic and disorderly. This can be proved by the fact that the binding energies of the AC edge tended to be weaker than those of the ZZ edge [45]. Therefore, it is more difficult for the AC surface to form stable functional group structures to resist the etching of high-energy oxygen atoms than the ZZ surface.

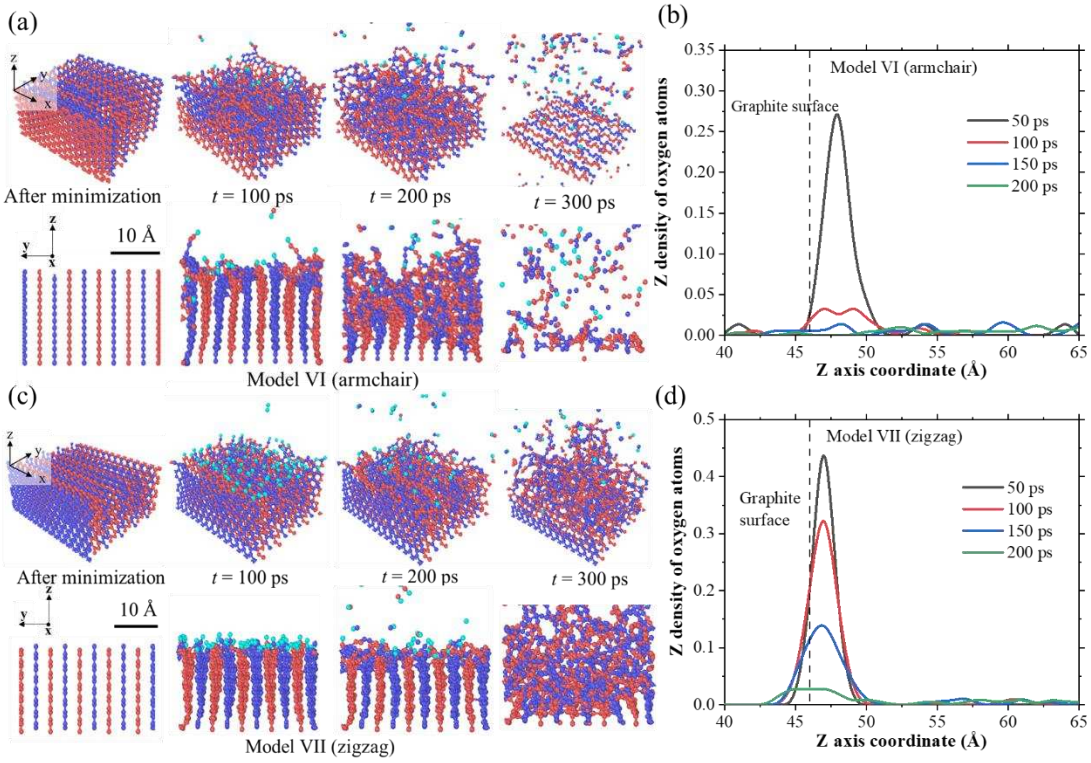

Figure 9 The snapshot illustrations of Model VI and VII with oxygen z-density analysis with the evolution of time.

Figure 10(a) shows the number of C-C bond broken for different layers with the evolution of time. The breaks of the C-C bond from the 1st layer to the 5th layer for

both Model VI and VII are observed to be gradually delayed and reach their maximums, proving the oxidative erosion of the basal planes being a 'layer by layer' phenomenon. The total number of broken C-C bond for Model VI grows exponentially from about 100 ps while that of Model VII grows exponentially from about 200 ps. The sequence of erosion events leads to the loss of C atoms from the graphite slabs, forming gas molecules as shown in **Figure 10(b)**. It is found that the starting time of gas generation for graphite with AC surface is earlier than that of graphite with ZZ surface. The mass fractions of O_2 and CO_2 for both Model VI and VII decrease gradually, while the mass fraction of CO increases rapidly during the catalytic ablation reaction. Later, the mass fraction of CO reaches its peak, while the mass fractions of O_2 and CO_2 molecules approach zero. Subsequently, the number of CO molecules starts to decrease while the number of C_2 molecules begins to increase rapidly. In the meanwhile, the mass fractions of C_3 and C_2O molecules increase slightly.

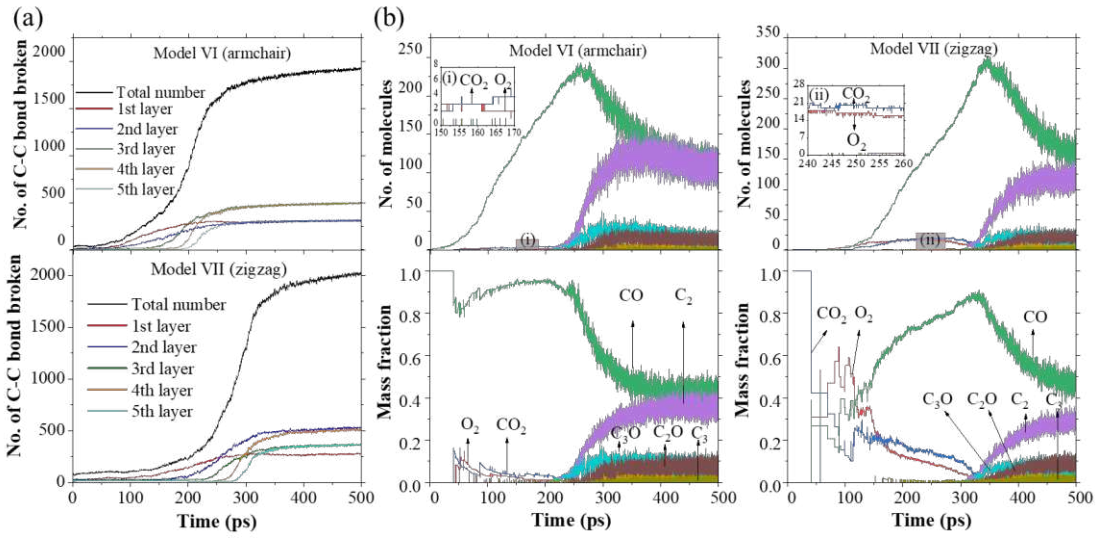

Figure 10 The C-C bond broken profiles and gasified component analysis as a function of time for Model VI and VII over time.

In order to compare the surface catalysis and ablation rate of the graphite slabs with different orientations, the catalysis recombination coefficients and the fraction of graphite C-C bond broken are obtained as shown in **Figure 11(b)**. Z-density of oxygen

atoms for Model VI decreases rapidly from 100 ps afterwards in **Figure 9(b)**, resulting in the catalytic recombination coefficient γ of Model VI smaller than that of Model VII, as shown in the **Figure 11(b)**. Besides, though all the surfaces can be etched by hyperthermal atomic oxygen with a layer by layer phenomenon, the armchair surfaces show the largest etching rate and basal presenting the lowest etching rage. It is clear from **Figure 11(a)** that an increase in system temperature causes a speedup of the graphite ablation process: Model VI with AC edge surface is ablated fastest with the largest C-C bond broken rate and the smallest catalytic recombination coefficient. Graphite with basal plane reveals better resistant to energetic oxygen atom etching compared to the graphite with AC edge surfaces and that with ZZ edge surfaces.

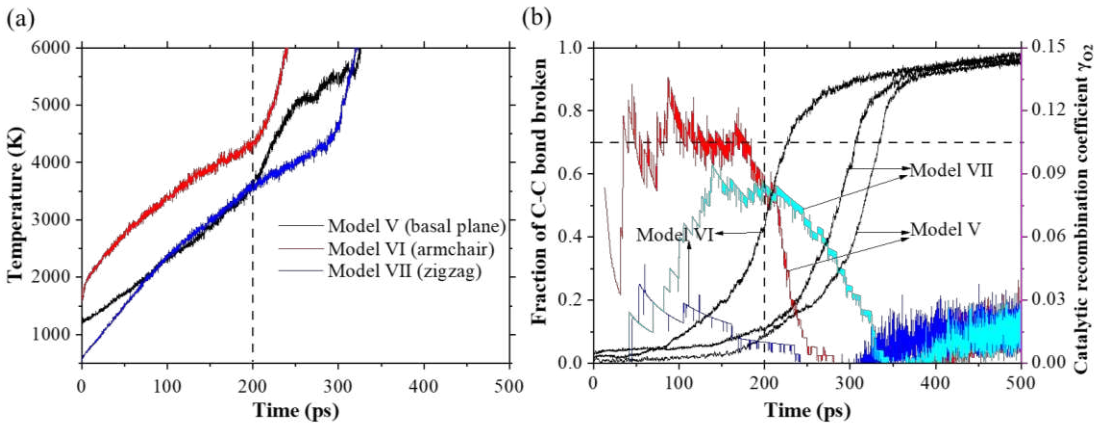

Figure 11 The system temperature profiles and the surface catalysis / ablation analysis as a function of time with the comparisons of Model V, VI and VII.

4. Conclusions

The surface catalysis and ablation processes of hyperthermal atomic oxygens colliding with graphite are simulated by MD method using ReaxFF reactive force field. The physical/chemical interactions between the hyperthermal atomic oxygens and the solid surface were investigated with seven models to study the effects of the oxygen energy flux density, the presence of multi layers beneath the graphene sheet surface and the graphite surfaces with different edges (graphite basal plane surface, AC edge surface

and ZZ edge surface). The simulation results can be concluded as followed:

(1) For all the seven models, the system temperature increases gradually due to the energy input to the system through the addition of successive oxygen atom impacts. The adsorption of oxygen atoms dominates at the beginning for all models when the temperature is relative low, generating O_2 molecules through the surface catalytic recombination of oxygen atoms. The ablation of graphene sheet accelerates while system temperature further going forward, along with the number of O_2 and CO_2 gas species declining gradually and forming the main incomplete oxidation production of CO gas molecules.

(2) The ablation rate of graphene surface accelerates significantly as oxygen energy flux density increases due to the higher system temperature resulting from the denser impingement of oxygen atoms. The traditional Arrhenius expression to describe the temperature effect on the surface catalysis process is inefficient due to the simultaneous ablation behavior.

(3) With the presence of multiple layers beneath the graphene sheet surface, the graphite slab can be etched by hyperthermal atomic oxygen with a layer by layer phenomenon. The more graphene stacks appearing below the top layer, the slower the ablation rate. This is due to the fact that additional graphene layers can act as a heat sink, slowing down the temperature rise by conduction due to oxygen-atom collisions.

(4) For graphite surfaces with different edges, the AC surfaces show the largest etching rate and basal presenting the lowest etching rage, revealing the fact that the binding energies of the AC edge tends to be weaker than those of the ZZ edge. Therefore it is more difficult for the AC surface to form stable functional group structures to resist the etching of high-energy oxygen atoms than the ZZ surface.

In the future, we will broaden our research through further exploring the temperature and pressure effects of both gas/solid phases on the surface catalysis and ablation behaviors with multiple carbon-based materials.

Acknowledgement

This research is supported by the National Numerical Wind Tunnel Project under the Grant NNW2018-ZT3A05.

References

[1] H. Lu, W. Chen, L. Yuan, W.-q. LIU, Ablation analysis and engineering calculation on carbon-based material of reentry vehicles, Journal of Ballistics 20(3) (2008) 107-110.

[2] P. Sanoj, B. Kandasubramanian, Hybrid carbon-carbon ablative composites for thermal protection in aerospace, Journal of Composites 2014 (2014).

[3] R.A. Dressler, Chemical Dynamics in Extreme Environments, World Scientific2001.

[4] K. Kratsch, L. Hearne, H. McChesney, Thermal performance of heat shield composites during planetary entry, Engineering Problems of Manned Interplanetary Exploration1963, p. 1515.

[5] R.D. Mathieu, Mechanical spallation of charring ablators in hyperthermal environments, AIAA journal 2(9) (1964) 1621-1627.

[6] R.B. POPE, N.S. VOJVODICH, Effect of gas composition on the ablation behavior of a charring material, AiAA Journal 2(3) (1964) 536-542.

[7] B. Holzknecht, An analytical model of the transient ablation of polytetrafluoroethylene layers, International Journal of Heat and Mass Transfer 20(6) (1977) 661-668.

[8] V.J. Murray, B.C. Marshall, P.J. Woodburn, T.K. Minton, Inelastic and reactive scattering dynamics of hyperthermal O and O2 on hot vitreous carbon surfaces, The Journal of Physical Chemistry C 119(26) (2015) 14780-14796.

[9] V.J. Murray, E.J. Smoll Jr, T.K. Minton, Dynamics of graphite oxidation at high temperature, The Journal of Physical Chemistry C 122(12) (2018) 6602-6617.

[10] K.T. Nicholson, T.K. Minton, S. Sibener, Temperature-dependent morphological evolution of HOPG graphite upon exposure to hyperthermal O (3P) atoms, Progress in organic coatings 47(3-4) (2003) 443-447.

[11] T. Ngo, E.J. Snyder, W.M. Tong, R.S. Williams, M.S. Anderson, O atom etching of graphite in low earth orbit, Surface Science 314(1) (1994) L817-L822.

[12] H. Kinoshita, M. Umeno, M. Tagawa, N. Ohmae, Hyperthermal atomic oxygen beam-induced etching of HOPG (0001) studied by X-ray photoelectron spectroscopy and scanning tunneling microscopy, Surface Science 440(1) (1999) 49-59.

[13] K.T. Nicholson, S. Sibener, T.K. Minton, Nucleation and growth of nanoscale to microscale cylindrical pits in highly-ordered pyrolytic graphite upon hyperthermal atomic oxygen exposure, High Performance Polymers 16(2) (2004) 197-206.

[14] V. Morón, P. Gamallo, R. Sayós, DFT and kinetics study of O/O 2 mixtures reacting over a graphite (0001) basal surface, Theoretical Chemistry Accounts 128(4-6) (2011) 683-694.

[15] V. Morón, L. Martin-Gondre, C. Crespos, P. Larregaray, P. Gamallo, R. Sayós, Classical dynamics study of atomic oxygen over graphite (0001) with new interpolated and analytical potential energy surfaces, Computational and Theoretical Chemistry 990 (2012) 132-143.
[16] V. Morón, L. Martin-Gondre, P. Gamallo, R. Sayós, Quasiclassical Trajectory Dynamics Study of Atomic Oxygen Collisions on an O-Preadsorbed Graphite (0001) Surface with a New Analytical Potential Energy Surface, The Journal of Physical Chemistry C 116(24) (2012) 13092-13103.
[17] V. Morón, L. Martin-Gondre, P. Gamallo, R. Sayós, Dynamics of the Oxygen Molecules Scattered from the Graphite (0001) Surface and Comparison with Experimental Data, The Journal of Physical Chemistry C 116(40) (2012) 21482-21488.
[18] J.T. Paci, H.P. Upadhyaya, J. Zhang, G.C. Schatz, T.K. Minton, Theoretical and Experimental Studies of the Reactions between Hyperthermal O(3P) and Graphite: Graphene-Based Direct Dynamics and Beam-Surface Scattering Approaches, The Journal of Physical Chemistry A 113(16) (2009) 4677-4685.
[19] K. Sendt, B.S. Haynes, Density functional study of the reaction of O2 with a single site on the zigzag edge of graphene, Proceedings of the Combustion Institute 33(2) (2011) 1851-1858.
[20] J.T. Paci, T.K. Minton, G.C. Schatz, Hyperthermal Oxidation of Graphite and Diamond, Accounts of Chemical Research 45(11) (2012) 1973-1981.
[21] J.T. Paci, I. Paci, Theoretical Studies of the Reactions between Hyperthermal O(3P) and Graphite: Holes and the Second Layer, The Journal of Physical Chemistry C 123(49) (2019) 29647-29655.
[22] B. Javvaji, P.R. Budarapu, V.K. Sutrakar, D.R. Mahapatra, M. Paggi, G. Zi, T. Rabczuk, Mechanical properties of Graphene: Molecular dynamics simulations correlated to continuum based scaling laws, Computational Materials Science 125 (2016) 319-327.
[23] J.-H. Zou, Z.-Q. Ye, B.-Y. Cao, Phonon thermal properties of graphene from molecular dynamics using different potentials, The Journal of chemical physics 145(13) (2016) 134705.
[24] F. Lin, Y. Xiang, H.-S. Shen, Temperature dependent mechanical properties of graphene reinforced polymer nanocomposites – A molecular dynamics simulation, Composites Part B: Engineering 111 (2017) 261-269.
[25] Y. Wang, Z. He, K.M. Gupta, Q. Shi, R. Lu, Molecular dynamics study on water desalination through functionalized nanoporous graphene, Carbon 116 (2017) 120-127.
[26] Y. Xia, Y. Xing, M. Li, M. Liu, J. Tan, Y. Cao, X. Gui, Studying interactions between undecane and graphite surfaces by chemical force microscopy and molecular dynamics simulations, Fuel 269 (2020) 117367.
[27] A.C. Van Duin, S. Dasgupta, F. Lorant, W.A. Goddard, ReaxFF: a reactive force field for hydrocarbons, The Journal of Physical Chemistry A 105(41) (2001) 9396-9409.
[28] C. Ashraf, A.C.T. van Duin, Extension of the ReaxFF Combustion Force Field toward Syngas Combustion and Initial Oxidation Kinetics, The Journal of Physical

Chemistry A 121(5) (2017) 1051-1068.
[29] D.A. Newsome, D. Sengupta, H. Foroutan, M.F. Russo, A.C. van Duin, Oxidation of silicon carbide by O2 and H2O: a ReaxFF reactive molecular dynamics study, Part I, The Journal of Physical Chemistry C 116(30) (2012) 16111-16121.
[30] S.G. Srinivasan, A.C.T. van Duin, P. Ganesh, Development of a ReaxFF Potential for Carbon Condensed Phases and Its Application to the Thermal Fragmentation of a Large Fullerene, The Journal of Physical Chemistry A 119(4) (2015) 571-580.
[31] S. Poovathingal, T.E. Schwartzentruber, S.G. Srinivasan, A.C.T. van Duin, Large Scale Computational Chemistry Modeling of the Oxidation of Highly Oriented Pyrolytic Graphite, The Journal of Physical Chemistry A 117(13) (2013) 2692-2703.
[32] S. Goverapet Srinivasan, A.C.T. van Duin, Direction dependent etching of diamond surfaces by hyperthermal atomic oxygen: A ReaxFF based molecular dynamics study, Carbon 82 (2015) 314-326.
[33] V.A. Ermakov, A.V. Alaferdov, A.R. Vaz, E. Perim, P.A. Autreto, R. Paupitz, D.S. Galvao, S.A. Moshkalev, Burning graphene layer-by-layer, Scientific reports 5 (2015) 11546.
[34] M. Majumder, K.D. Gibson, S.J. Sibener, W.L. Hase, Chemical Dynamics Simulations and Scattering Experiments for O2 Collisions with Graphite, The Journal of Physical Chemistry C 122(28) (2018) 16048-16059.
[35] X.Y. Liu, F.C. Wang, H.S. Park, H.A. Wu, Defecting controllability of bombarding graphene with different energetic atoms via reactive force field model, Journal of Applied Physics 114(5) (2013) 054313.
[36] Z. Bai, L. Zhang, L. Liu, Bombarding Graphene with Oxygen Ions: Combining Effects of Incident Angle and Ion Energy To Control Defect Generation, The Journal of Physical Chemistry C 119(47) (2015) 26793-26802.
[37] Q. Qiao, C. Liu, W. Gao, L. Huang, Graphene oxide model with desirable structural and chemical properties, Carbon 143 (2019) 566-577.
[38] M. Majumder, H.N. Bhandari, S. Pratihar, W.L. Hase, Chemical dynamics simulation of low energy N2 collisions with graphite, The Journal of Physical Chemistry C 122(1) (2018) 612-623.
[39] N.A. Mehta, V.J. Murray, C. Xu, D.A. Levin, T.K. Minton, Nonreactive scattering of N2 from layered graphene using molecular beam experiments and molecular dynamics, The Journal of Physical Chemistry C 122(18) (2018) 9859-9874.
[40] K. Yoon, A. Ostadhossein, A.C.T. van Duin, Atomistic-scale simulations of the chemomechanical behavior of graphene under nanoprojectile impact, Carbon 99 (2016) 58-64.
[41] C. Zhang, A.C.T. van Duin, J.W. Seo, D. Seveno, Weakening effect of nickel catalyst particles on the mechanical strength of the carbon nanotube/carbon fiber junction, Carbon 115 (2017) 589-599.
[42] V.J. Murray, L. Zhou, C. Xu, Y. Wang, H. Guo, T.K. Minton, Scattering Dynamics of Glycine, H2O, and CO2 on Highly Oriented Pyrolytic Graphite, The Journal of Physical Chemistry C 123(6) (2019) 3605-3621.

[43] K. Chenoweth, A.C. Van Duin, W.A. Goddard, ReaxFF reactive force field for molecular dynamics simulations of hydrocarbon oxidation, The Journal of Physical Chemistry A 112(5) (2008) 1040-1053.
[44] S. Goverapet Srinivasan, A.C. van Duin, Molecular-dynamics-based study of the collisions of hyperthermal atomic oxygen with graphene using the ReaxFF reactive force field, The Journal of Physical Chemistry A 115(46) (2011) 13269-13280.
[45] Q. Ly, B.V. Merinov, H. Xiao, W.A. Goddard III, T.H. Yu, The oxygen reduction reaction on graphene from quantum mechanics: comparing armchair and zigzag carbon edges, The Journal of Physical Chemistry C 121(44) (2017) 24408-24417.